The use of novel digital image analysis technique and Theological tools to characterize nanofiber nonwovens

Wannes Sambaer[a], Martin Zatloukal[a,*], Dusan Kimmer[b]

A B S T R A C T

Polyurethane (PU) solved in dimethylformamide (DMF) was electrospun under one set of conditions using five different supporting textiles. The mechanical properties of the nanofiber mats were measured by the Sentmanat extensional rheometer, and the pore size distribution was calculated by a newly proposed digital image analysis methodology applied on nanoscale SEM images taking macroscopic features of the nonwovens into account. It has been found that supporting textiles have a very high effect on mechanical properties of nanofiber mats (even if their fiber diameter distributions are similar), which can be explained by different porosity of the prepared samples.

1. Introduction

In recent years, nanofiber-related research work, publications and patents have grown rapidly in areas of biological, medical, filtration, sensors, composites and catalysis applications [1-3]. One of the most popular techniques for nanofiber production is electrospinning where the polymer solution is stretched by the electrostatic

force acting between two electrodes with simultaneous evaporation of the solvent [4,5]. In this case, the produced nanofibers are accumulated on a grounded collector, which is covered by the supporting textile. It has been found that the final properties of the produced nanofiber nonwovens depends on the material-related properties, such as polymer type, viscosity, electrical conductivity [6], surface tension of the solvent, as well as on the processing-related characteristics, such as applied voltage [7], distance between collector and electrode, humidity [8,9], pressure [10] and temperature [10] in the chamber. One of the most important characteristic of polymeric nanofiber webs are

their mechanical properties and, therefore, it is not surprising that considerable effort has been paid to experimentally determining these characteristics by using conventional tensile machines or more sophisticated equipment such as an atomic force microscope cantilever (AFM) or bending tests [8,11-15]. Even if many useful conclusions about the link between processing parameters and produced nanofiber webs can be extracted from the open literature, to our knowledge, there is no research related to the role of the supporting textile type (where the nanofibers are collected during the electrospinning process) on the product properties. Therefore, in this work, the role of the supporting textile type on the mechanical and structural characteristics of the nanofiber nonwovens will be investigated in detail. For this purpose, firstly, a specific procedure to measure mechanical properties of the nanofiber webs by using a Sentmanat extensional rheometer [16-18] will be utilized to overcome difficulties connected with problematic manipulation of extremely small fibers, and very sensitive force transducer requirements. Secondly, a novel digital image analysis technique (which is based on the theoretical approach proposed in [19-21]) will be developed and used for the detailed structure nanofiber web analysis.

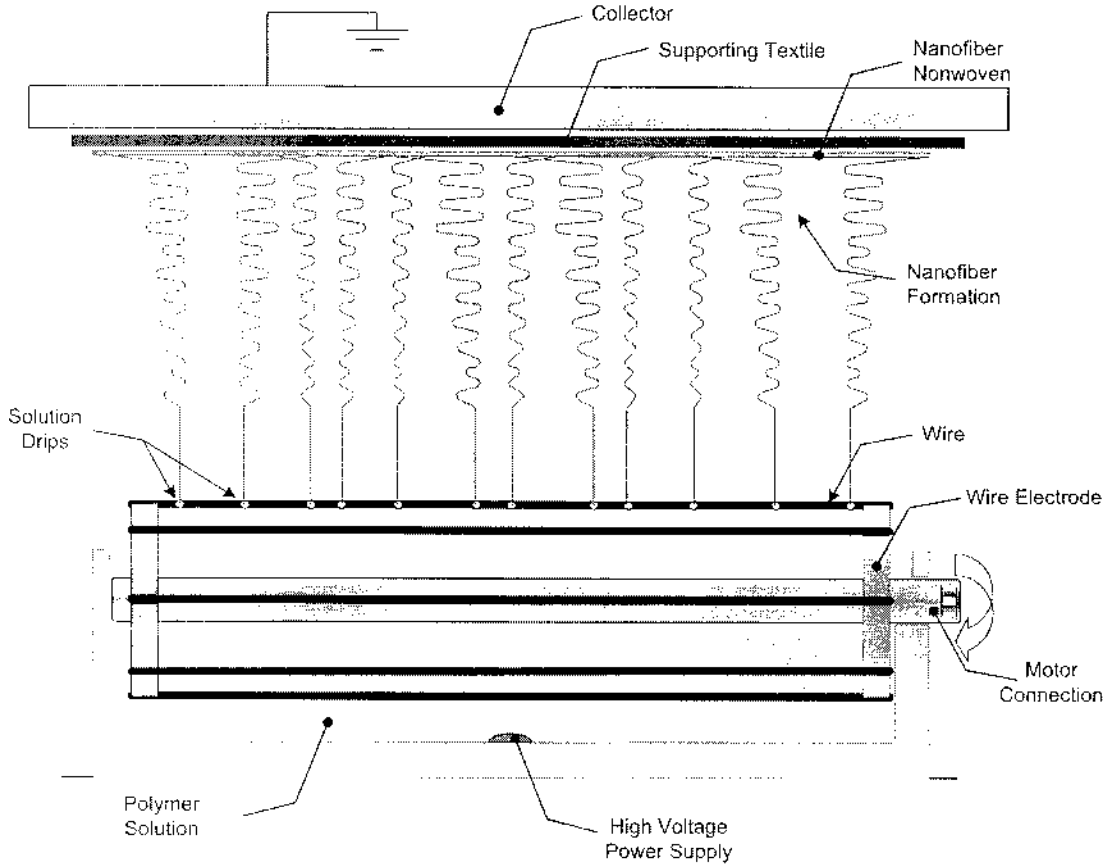

Fig. 1. Scheme of the electrospinning process.

2. Experimental and theoretical analysis

2.1 Material

A polyurethane (PU) solution based on 4,4'methylene-bisphenylisocyanate, poly(3-methyl-l,5-pentanediol)-alt- (adipic, isophtalic acid) and 1,4 butanediol (molar ratio 6:1:5) solved in dimethylformamide (DMF) was synthesized. The prepared solution was suitable for electrospinning and had a PU concentration of 11.5 wt%, viscosity of 0.99 Pa s and conductivity of 151 jiS/cm (adjusted by tetraethylamonium bromide).

2.2. *Sample preparation by electrospinning process*

PU nanofibers were prepared from the above mentioned PU solution with a commercially available NanoSpider™ machine (Elmarco s.r.o. Liberec, Czech

Table 1
Detailed characteristics of the used supporting textiles.

Textile	% Poly(m-aramid)	Staple length (mm)	Fineness (dtex)	Fibre diameter (μm)
311	89.9%	51	1.7	12.5
318	35.0%	51	1.7	12.5
319	98.8%	51	1.7	12.5
	% Poly(p-aramid)	Staple length (mm)	Fineness (dtex)	Fibre diameter (μm)
311	90.0%	–	1.7	12.7
318	63.8%	50	2.2	13.8
319	–	–	–	–
	% Stainless steel	Staple length (mm)	Fineness (dtex)	
311	1.2%	–	400	
318	1.2%	51	400	
319	1.2%	51	400	
PPNW	Melt blown PP 30 g/m²	Freshening Polyfix N		
PPPE	Melt blown PP + PE foil	Freshening Polyfix N		

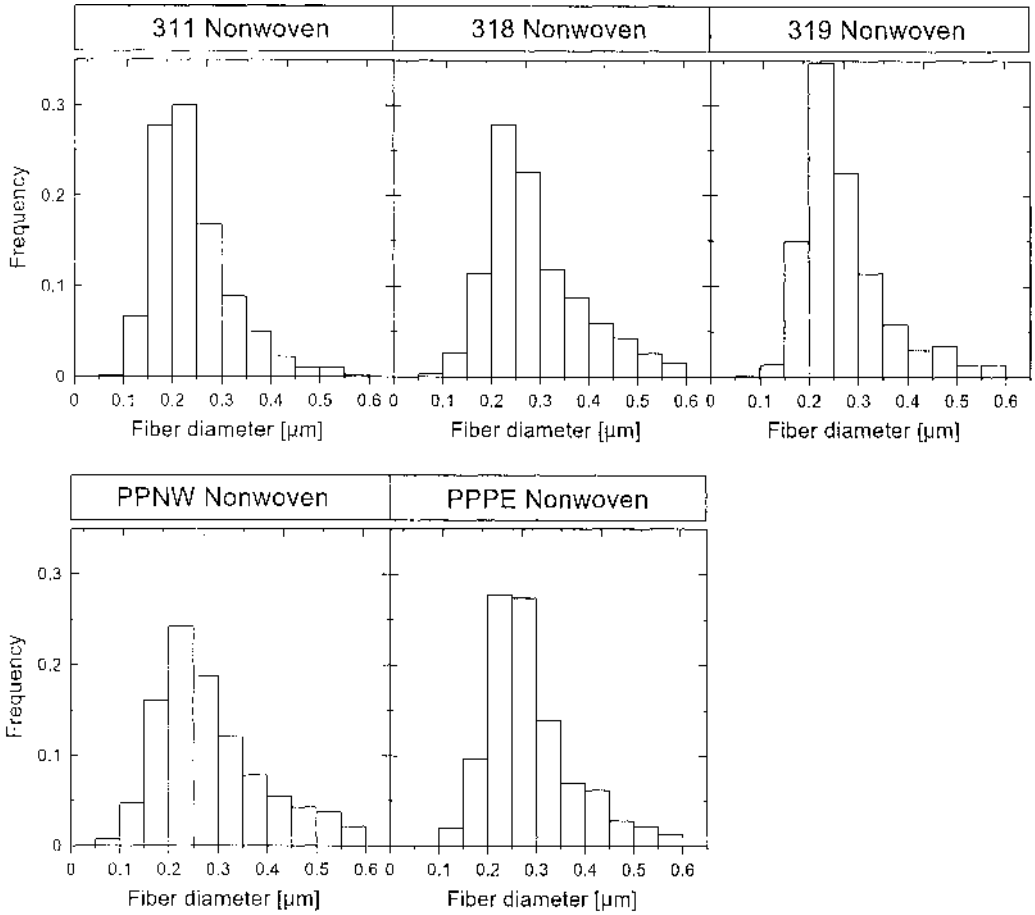

Fig. 2. Fiber diameter distributions for all investigated nanofiber nonwovens.

Republic, http://www.elmarco.com/) equipped with one rotational electrode (see Fig. 1) and five different supporting textiles. Three of them were based on meta and para aramid fibers containing 1.2% of stainless steel fibers (which were woven through these textiles) whereas the other two were based on melt-blown polypropylene with and without polyethylene foil (see Table 1 for more details). The experimental conditions were: relative humidity 28%, temperature 27.5 °C, electric voltage between wire rotational electrode and grounded collector (electrode) 75 kV, distance between electrodes 180 mm, rotational electrode speed 7 rpm and speed of supporting textile collecting nanofibers was 0.16 m/min. Samples for further analyses were taken from the middle part of the produced nanofiber textiles having the fiber diameter distribution as depicted in Fig. 2.

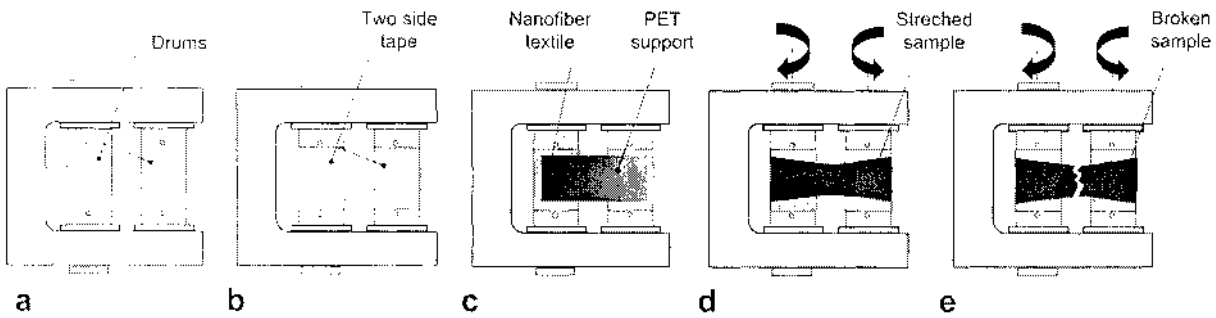

Fig. 3. Visualized methodology for the tensile testing of the nanofiber nonwoven by using Sentmanat extensional rheometer, a) SER unit, b) SER with double- sided adhesive tape, c) Nanofiber web deposition on the SER unit, d) Sample stretching, e) Sample at break.

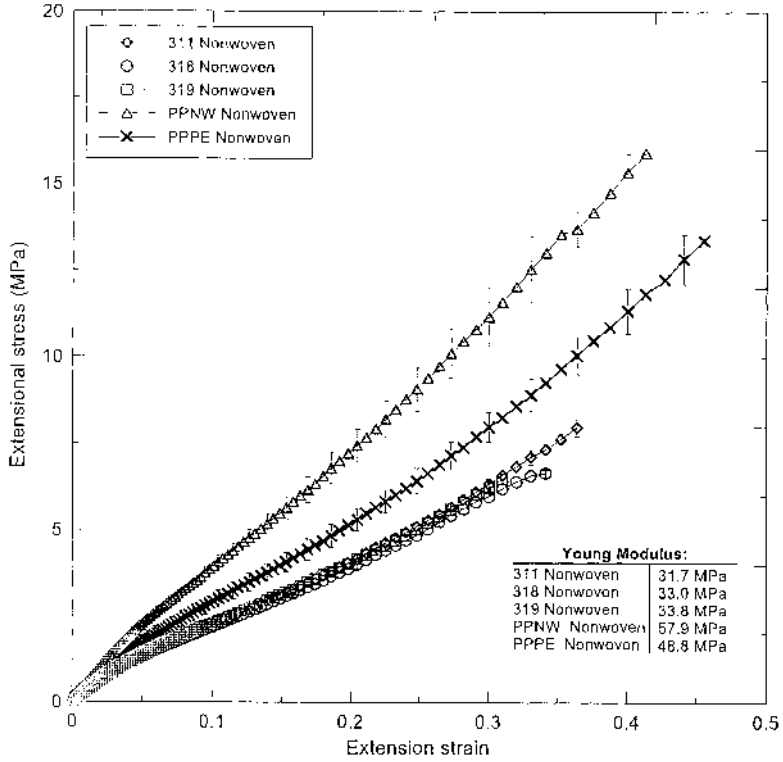

Fig. 4. Measured extensional stress as a function of extensional strain for all investigated nonwoven samples.

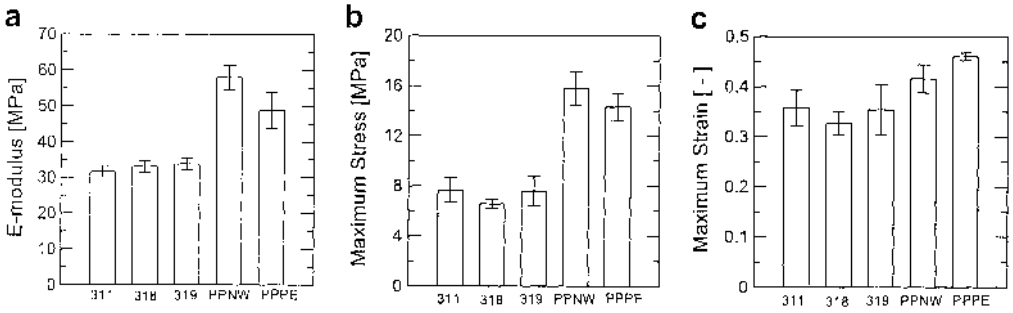

Fig. 5. Summarized tensile strength characteristics for all investigated nonwoven samples, a) E-modulus, b) Stress at break, c) Strain at break.

Table 2
Summarization of mechanical properties for different PU nanofiber nonwovens produced on different supporting textiles.

Sample name		E-modulus [MPa]	Max Stress [MPa]	Max Strain [–]
311 nonwoven	Average	31.7	7.7	0.358
	Deviation	1.6	1.0	0.035
	Fault	5.1%	12.7%	9.8%
318 nonwoven	Average	33.0	6.6	0.3
	Deviation	1.7	0.4	0.024
	Fault	5.2%	5.5%	7.3%
319 nonwoven	Average	33.8	7.6	0.4
	Deviation	1.5	1.2	0.0
	Fault	4.5%	15.4%	14.0%
PPNW nonwoven	Average	57.9	15.8	0.416
	Deviation	3.4	1.4	0.028
	Fault	5.9%	8.7%	6.7%
PPPE nonwoven	Average	48.8	14.3	0.460
	Deviation	5.1	1.1	0.008
	Fault	10.4%	7.8%	1.7%

2.3. *Tensile testing*

An Advanced Rheometric Expansion System (ARES) rotational rheometer equipped with Sentmanat Exten- sional Rheometer (SER) Universal Testing Platform [16-18], Fig. 3a, (which is normally used for polymer melt extensional viscosity/strength characteristics determination) was used in this work to determine mechanical properties of the prepared nanofiber textiles. For this purpose, the following strategy has been proposed. Firstly, double-sided adhesive tape was stuck on both SER drums (Fig. 3b). Secondly, the very thin nanofiber textile (deposited on PET foil) was attached on this tape and then the PET foil was carefully removed (Fig. 3c). Finally the sample was stretched at a constant extensional strain rate of 0.01 s^{-1} (Fig. 3d) until the sample breaks (Fig. 3e). The

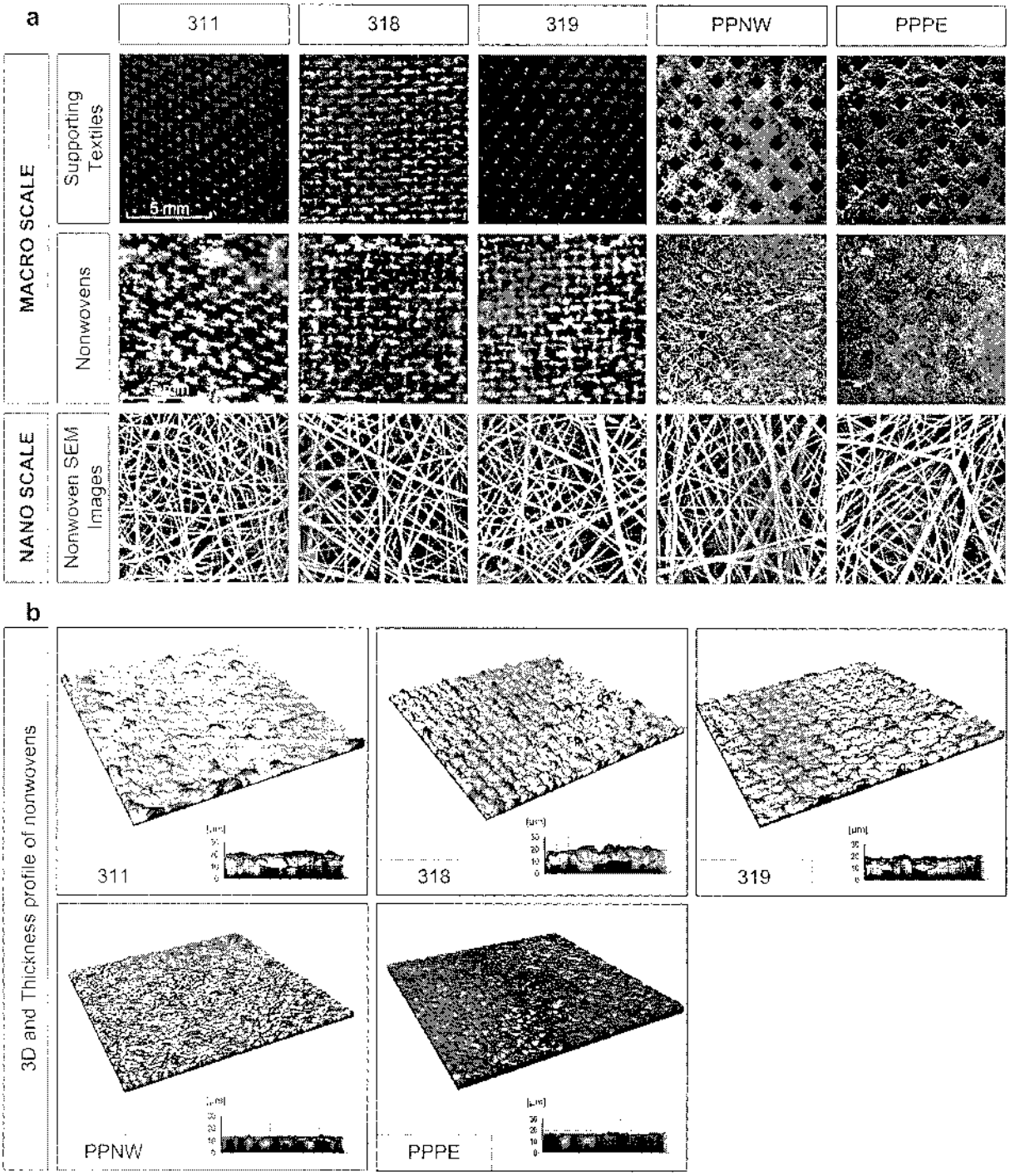

Fig. 6. Visualization of the utilized supporting textiles and obtained nanofiber nonwovens through electrospinning process, a) Macroscale top view of the used supporting textiles and obtained nanofiber nonwovens together with nanoscale views, b) Visualized macroscale view of 3D structure and thickness profile for obtained nanofiber nonwoven.

obtained tensile curves (extensional stress as a function of extensional strain) and basic characteristics such as Young's modulus and stress/strain at break are depicted in Figs. 4 and 5 and summarized in Table 2 for all tested samples. As it can be seen, there is a big difference between the mechanical properties of the nanofiber nonwovens due to different supporting textiles that were used during the electrospinning process. In more detail, PU nanofiber samples where the melt blown PPNW and PPPE supporting textiles were used have much higher

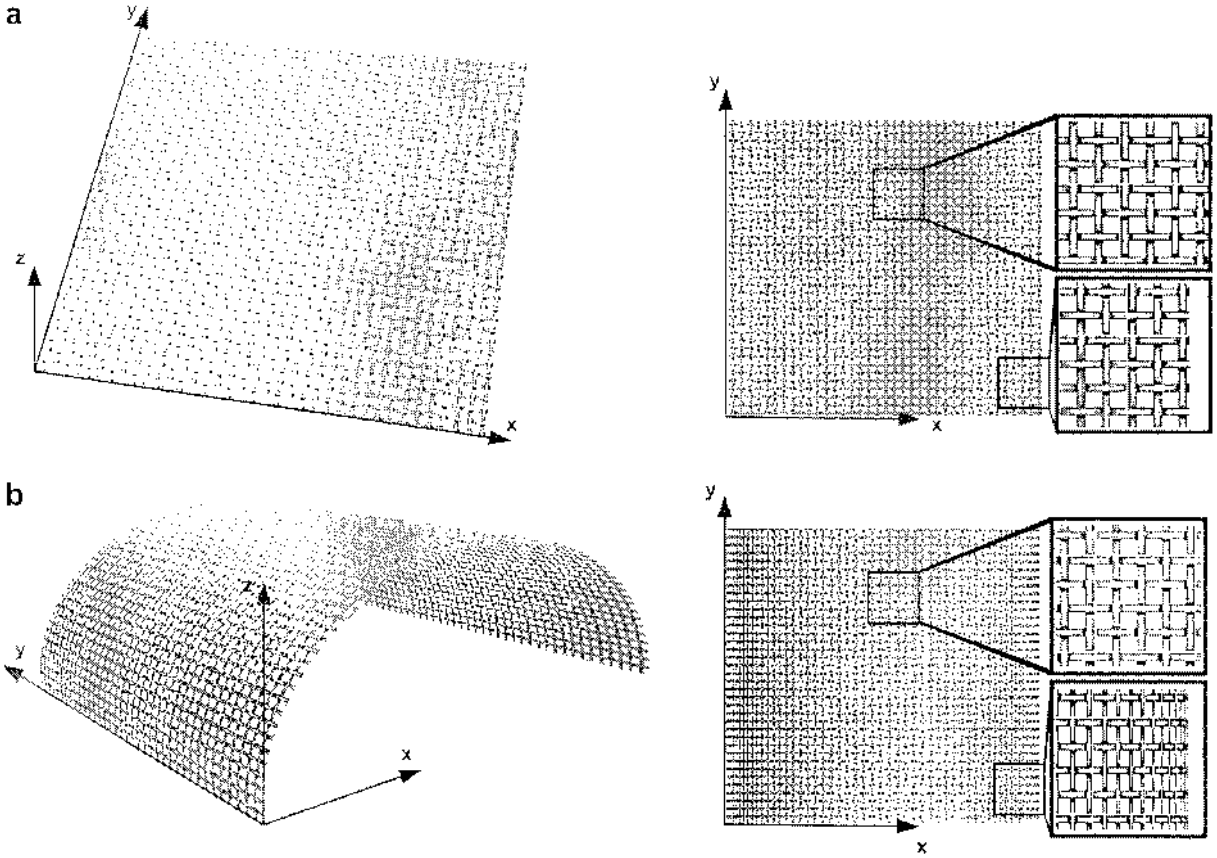

Fig. 7. Effect of the surface bending on the artificial change of the pore sizes if only top view is considered, a) Flat sample surface, b) Bended sample surface.

Young's modulus and stress/strain at break in comparison with PU nanofiber samples which have been produced on supporting textiles 311, 318 and 319 (based on aramid). From this experimental data, it is obvious that the supporting textile used during the electrospinning process has crucial impact on the final mechanical properties of the PU nanofiber nonwoven material. An interesting question is why the supporting textile has such a high effect on the final mechanical properties of the produced nonwovens having similar and/or comparable fiber diameter distribution (see Fig. 2). In order to understand this phenomenon in more detail, we have developed and used a novel digital image analysis technique to determine pore size distribution for all tested samples, which is introduced in the next section.

With respect to mechanical testing by using SER, it should be mentioned that the main advantage of this 'rheology based' methodology is the possibility to measure

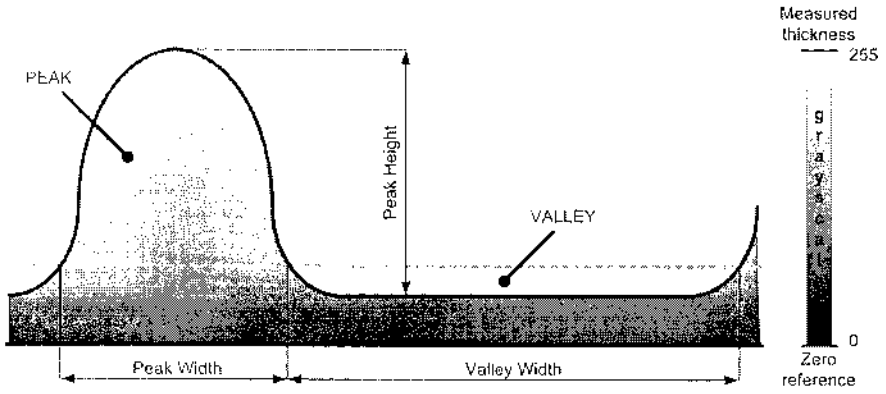

Fig. 8. Definition of 3D structure characteristics such as peak height, peak width and valley width for 'correct' threshold level calculation.

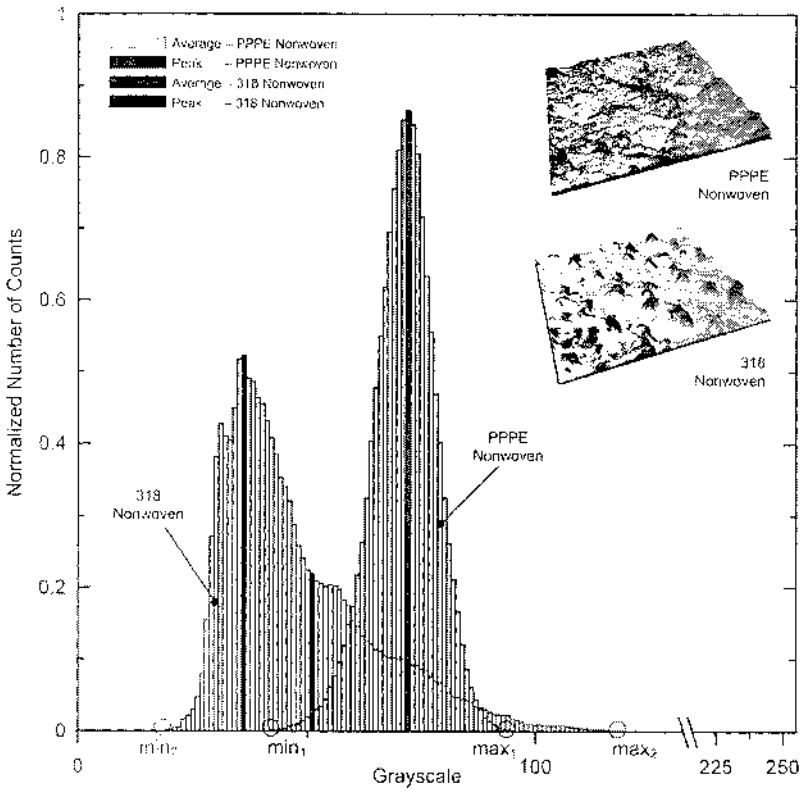

Fig. 9. Normalized greyscale histogram for PPPE and 318 nonwovens.

very fine structures with low experimental error due to the utilization of very sensitive torque/normal force transducers, which are normally present on standard rotational rheometers for polymer melt rheology evaluation. Moreover, the measurements can be done at different exten- sional strain rates and temperatures by using the conventional rheometer oven, which is difficult or impossible to do by using standard methodologies.

2.4. *Nanofiber based nonwovens structure analysis*

In Fig. 6a, macroscale as well as nanoscale views of both supporting textiles and corresponding PU nanofiber based nonwovens are provided. It is clearly visible that the specific 3D character of the supporting textile texture is 'copied' into the PU nanofiber based nonwovens as it is visible on the macroscale pictures. In more detail, it is clearly visible that the use of the aramid based supporting textiles during the electrospinning process causes creation of highly 3D textured nonwovens (with high number of peaks and valleys), whereas the use of melt blown supporting textiles leads to generation of more 2D textures (the thickness profile of PU nonwovens is more even in this case), as visible in Fig. 6b. This 3D nature of the nonwoven texture may cause an artificial pore size density increase as demonstrated in the example Fig. 7. In this Figure, 2D top views of two identical virtual rectangular textiles (having different 3D textures) are provided.

In Fig. 7a, the textile having identical pore sizes and flat surface is depicted. On the other hand, the Fig. 7b shows top view of exactly same textile which is bent i.e. surface is not flat. Even if the pore sizes are identical in both cases, due to the textile bending (peak occurrence), artificial decrease of the pore sizes can occur, as visible in Fig. 7b. This means that the 3D nature of any analyzed nanofiber based nonwovens has to be taken into account for detailed structure analysis, especially if a Scanning Electron Microscope (SEM) picture representing the top view of the sample is utilized. Note that all SEM pictures used in this work were obtained by using field emission scanning electron microscopy (Vega II LSU, Tescan, Czech republic). The analyzed nanoscale pictures had a resolution of 9009 x 9009 px where one pixel represents a square of 10 by 10 nm.

2.4.1. 3D correction for nanoscale SEM pictures

At the beginning, it is necessary to relate greyscale level of the macroscale pictures with the real sample thickness. To do that, the nonwoven samples were scanned with black paper on top to increase the contrast of the picture. The black color of the paper (greyscale number is equal to 0) was taken as a zero-reference thickness of the nanofiber textile whereas the brightest point (greyscale number up to 255) was calibrated as the maximum thickness, which was measured with a micrometer on the real nonwoven sample. By using these two calibration points, the whole

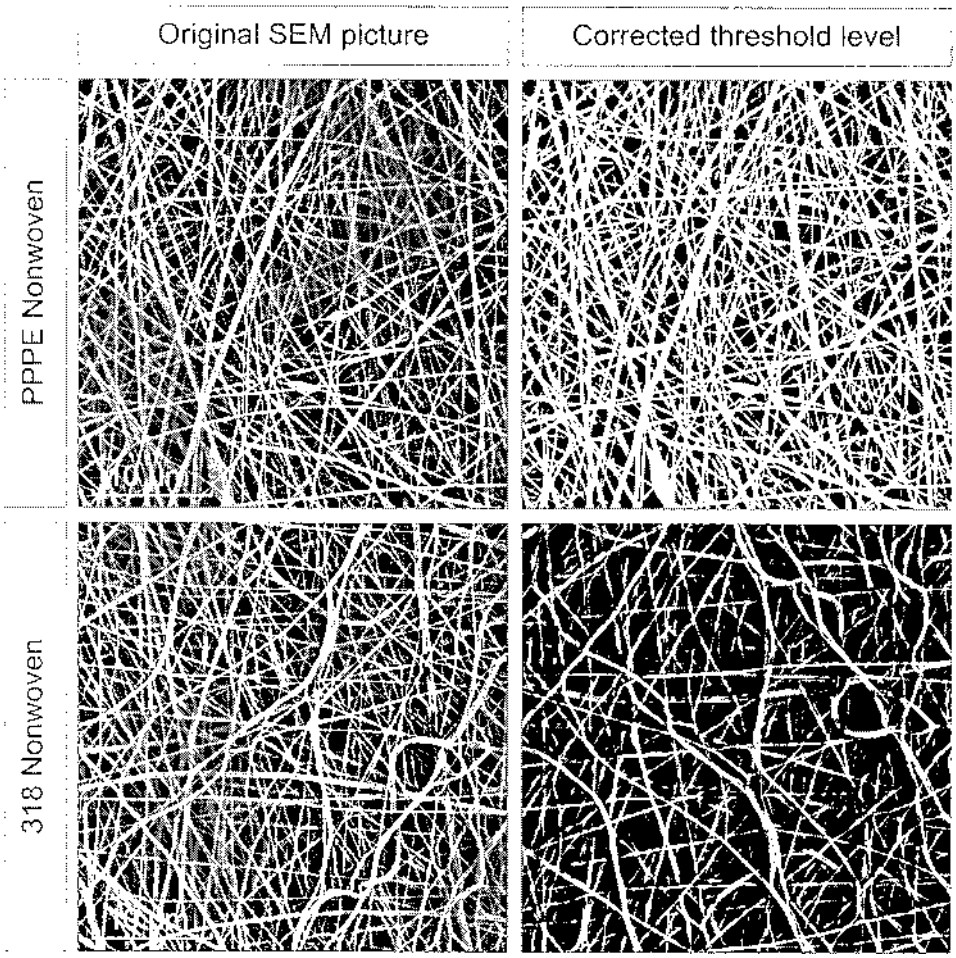

Fig. 10. SEM pictures for flat PPPE and 3D 318 nonwoven samples before and after 'correct' threshold level x application.

range of the greyscale values has been related to the thickness, considering a linear relationship between these two variables.

The basic principle of the 3D correction is modification of 2D SEM pictures to emphasize all structure details at one real depth level, which will be the same for all investigated samples. This can be done by defining the 'correct' threshold level x (pixels having greyscale value higher or lower than threshold level value becomes white or black, respectively) for each 2D SEM picture by using the following 3D structure characteristics: the peak height, ¡3, and the peak and valley width ratio *a* (graphical definition of these parameters is provided in Fig. 8). All these parameters can be determined from the calibrated macroscale picture greyscale histogram as is demonstrated in the following example. Fig. 9 shows two different greyscale histograms (pixel greyscale value distribution) for a macroscale flat structure (PPPE sample) and a 3D structure (318 sample). Each histogram is characterized by the following values: minimum, *min*, maximum, *max*, the most frequent, P, and average, ¡JL, greyscale numbers. By using these parameters, the 'correct' threshold level % (which can vary only between 0 and 255) can be determined from the peak height (Eq. (1)) and the peak and valley width ratio *a* (Eq. (2)) according to Eq. (3).

$$\beta = \max - \min \tag{1}$$

$$\alpha = \frac{P}{\mu} \tag{2}$$

$$\chi = \frac{\beta}{\alpha} \tag{3}$$

where the average greyscale number ,is defined as following:

$$\mu = \frac{\sum_{i=0}^{255} iC_i}{\sum_{i-0}^{255} C_i} \tag{4}$$

Here, *i* is the greyscale number and *Q* represents number of counts for the ith greyscale number.

It also should be mentioned that original SEM pictures may have different lightening depending on the operator and microscopy type. In order to have comparable SEM

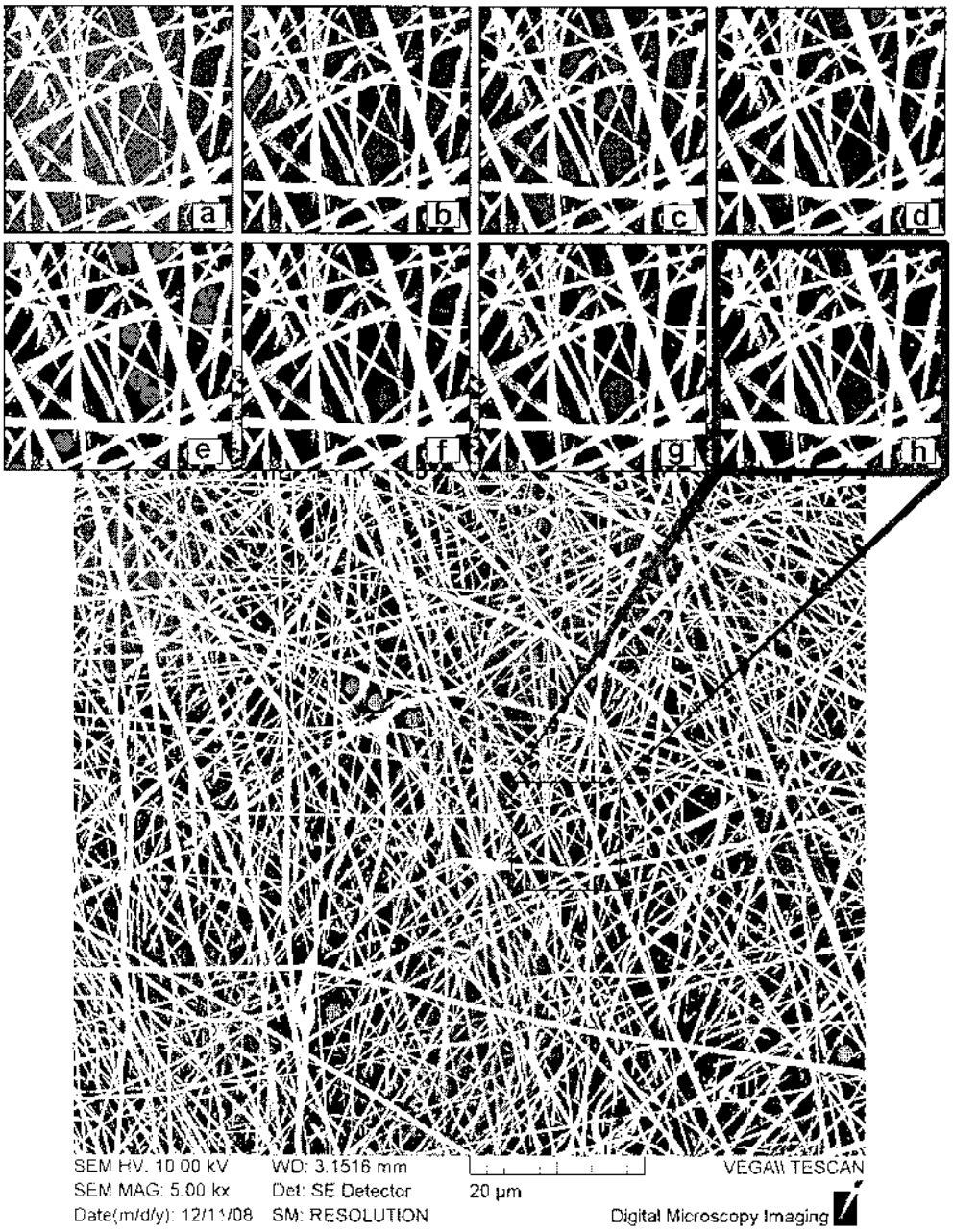

Fig. 11. Visualization of pore size distribution analysis for PPNW nonwoven sample for different circle diameters: D_A = 250nm. D_B = 450nm, D_C = 650 nm, D_D = 850 nm, D_E = 1050 nm, D_F = 1250 nm, D_G = 1650 nm, D_H = 1850 nm.

picture lightening, firstly, average greyscale level for each picture has been evaluated from the greyscale histogram. Secondly, the obtained individual average greyscale values for each picture have been averaged to get one total greyscale value average. Finally, the lightness for ail SEM pictures has been changed in such a way, that ail the pictures have the same average greyscale number, which is equal to the total greyscale value average. After this procedure, the 'correct' threshold level % has been applied for all SEM pictures to perform pore size distribution analysis, which is described below in more detail (see Fig. 10 that shows SEM pictures for flat PPPE and 3D 318 samples before and after 'correct' threshold level *x* application).

2.4.2. Pore size distribution analysis

In this part, novel Scanning Electron Microscope (SEM) picture digital image analysis technique for determination of pore size distribution for nanofiber based nonwovens is introduced. This method is based on the recent work of

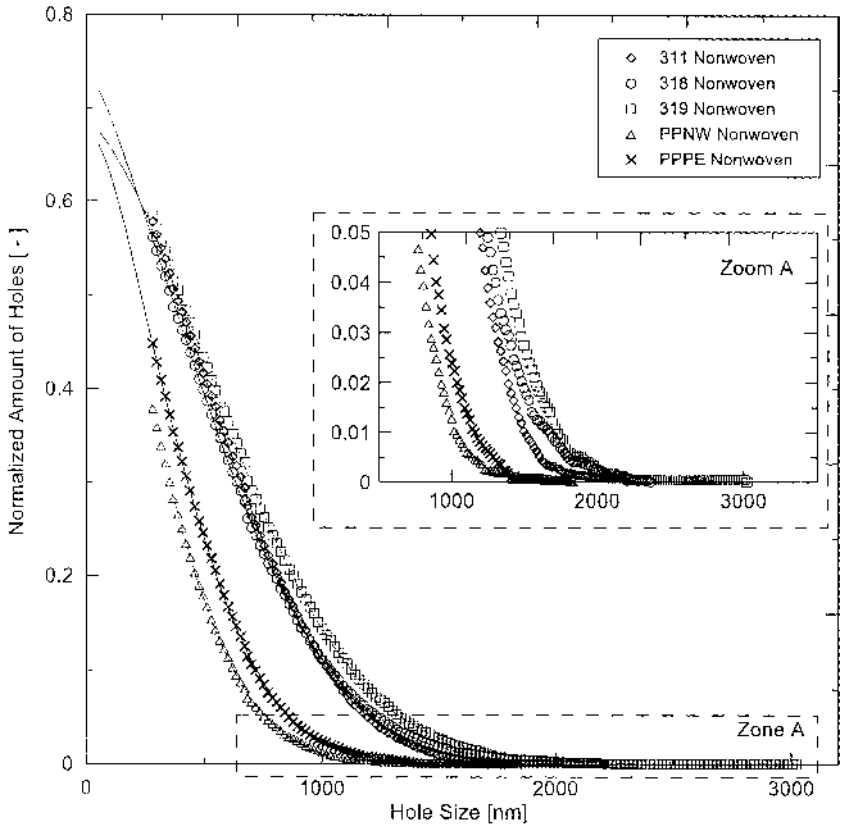

Fig. 12. Normalized amount of holes as a function of the hole size for all samples where symbols represents raw data and lines represents prediction of double stretched exponentional (Kohlrausch-Williams-Watts) function.

Ghasemi-Mobarakeh and Semnani et al. [20,21], who analyze the pores by using different cells with three different characteristic sizes (10, 20 and 30 \xm) that could infiltrate the fiber based product. In this work, we have generalized this approach considering virtually unlimited number of cells (depends on particular computer memory allocation capability of the PC used) having sizes from units of nanometers to hundreds of fim which can pass through the fiber nonwoven, and also taking the 3D macroscopic shape of the nanofiber based textile properly into account through application of 'correct' threshold level %. In Fig. 11, a part of the graphical results are shown to demonstrate how the methodology works. After this procedure is done, the number of circles has been counted and normalized for each sample and plotted versus circle diameter, which represents the pore/hole size in this case (see Fig. 12). In order to calculate pore/hole size distribution curve, the derivatives from the Fig. 12 has to be calculated. To do that effectively and precisely, the data in Fig. 12 were fitted by a combination of two stretched exponentional functions (Kohlrausch-Wil- liams-Watts, KWW, function) having the following form:

$$N(D) = A_1 \exp\left[-\left(\frac{D}{\tau_1}\right)^{\beta_1}\right] + A_2 \exp\left[-\left(\frac{D}{\tau_2}\right)^{\beta_2}\right] \qquad (5)$$

where JV(D) is normalized number of holes, D is the hole size in nm and $A\backslash$, $A2$, Pi, $2>$ and 12 are fitting constants.

As can be seen in Fig. 12, the chosen model (solid line in this Figure) describes the discrete data very well and, thus, the normalized derivative dJV(D) = d(normalized number of holes)/d(hole size) can be easily calculated from Eq. (5) by using the following expression:

$$\frac{dN(D)}{} = \frac{A_1 \exp\left[-\left(\frac{D}{\tau_1}\right)^{\beta_1}\right]\frac{\beta_1}{\tau_1}\left(\frac{D}{\tau_1}\right)^{\beta_1 - 1} + A_2 \exp\left[-\left(\frac{D}{\tau_2}\right)^{\beta_2}\right]\frac{\beta_2}{\tau_2}\left(\frac{D}{\tau_2}\right)^{\beta_2 - 1}}{A_1 \exp\left[-\left(\frac{D_s}{\tau_1}\right)^{\beta_1}\right] + A_2 \exp\left[-\left(\frac{D_s}{\tau_2}\right)^{\beta_2}\right]} \qquad (6)$$

where D_s is a constant equal to the smallest (circle/hole) diameter that can be detected in the picture. The obtained pore size distribution curves for all investigated samples are depicted in Fig. 13. For the pore size distribution curves evaluation, D_{z+1} hole size average (which is sensitive to the highest pores in the analyzed structure), which is defined below has been used

$$D_{z+1} = \frac{\int_{D_s}^{\infty} D^3 dN(D) dD}{\int_{D_s}^{\infty} D^2 dN(D) dD} \qquad (7)$$

Based on the pore size distribution curves depicted in Fig. 13, it can be concluded that the use of melt blown supporting textiles during electrospinning process leads

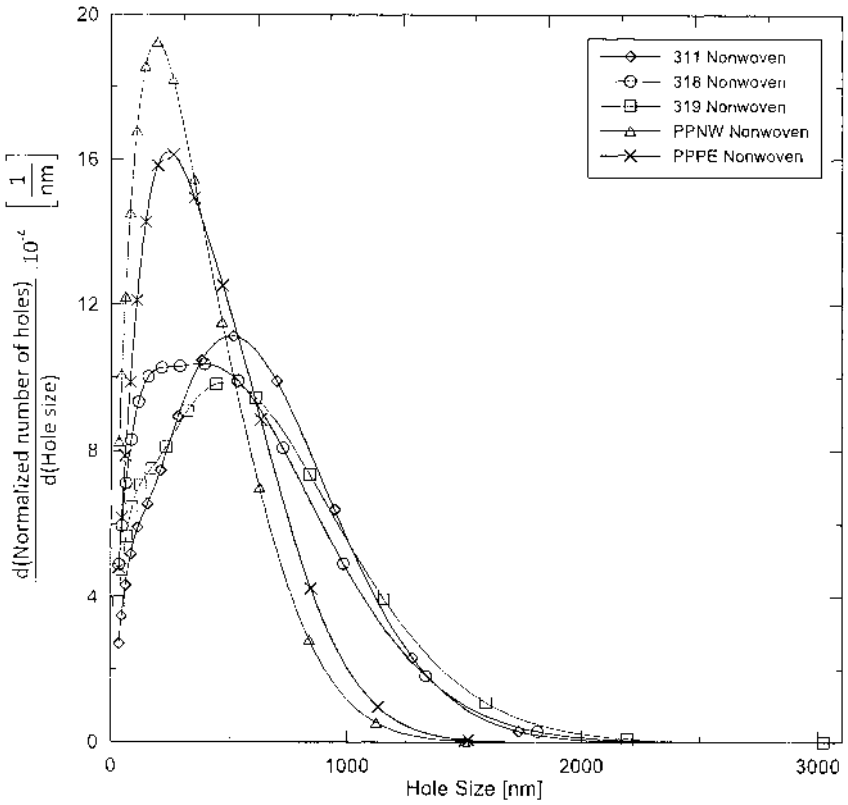

Fig. 13. Calculated pore size distribution for all investigated nonwoven samples.

to nanofiber based structures (PPNW and PPPE samples) having much smaller pores than structures prepared by the use of the aramid based supporting textiles (311, 318, 319 samples). For experimental determination of the amount of air in the mats, the air or porosity factor $a = 1 - (Pf/Ppu)$ has been utilized, where pf and *ppy* are densities of fibers and bulk PU, respectively. The density of the fibers was determined from 10 different measurements of the weight and the volume for each sample. Volume has been calculated from the rectangle sample area (width = 12.7 mm, length = 50 mm) and sample thickness. Note that percentage amount of the air has also been theoretically evaluated from area calculation between all nanofibers by using the circles having the smallest possible size, i.e. one pixel size, for all investigated samples. Theoretically, as well as experimentally, determined amounts of air are summarized for all samples in Table 3. Clearly, the samples having the smallest pores (PPNW and PPPE) contain less air than samples having the higher pores (311, 318, 319). It can also be seen that the error of measured amount of air is much higher than the theoretical one due to thickness measurement difficulties (small sample thicknesses and high elasticity). The airfactor difference between investigated samples prepared from the same PU solution can explain their big differences in mechanical properties because the amount of PU material in each sample is different. This is visible in Figs. 14 and 15 where the maximum stress at break together with E-modulus is plotted as a function of D_{z+1} hole size average and percentage amount of air.

3. Conclusions

Based on the performed experimental work and proposed novel digital image analysis technique for nanoscale SEM pictures (taking macroscopic structure features into account) has been found that supporting textiles have very high effect on mechanical properties of polyurethane nanofiber nonwovens prepared by the electrospinning process (even if their fiber diameter distributions were similar), which can be explained by different porosity of the prepared samples.

Table 3
Theoretically as well as experimentally determined airfactor for all investigated nonwoven samples.

Nonwoven	Experimental Airfactor	Theoretical Airfactor
311	84.9% ± 3.7%	79.1% ± 1.3%
318	83.9% ± 4.1%	68.7% ± 0.2%
319	83.8% ± 4.5%	73.5% ± 1.7%
PPNW	75.5% ± 2.9%	34.1% ± 0.9%
PPPE	79.0% ± 9.4%	43.5% ± 0.5%

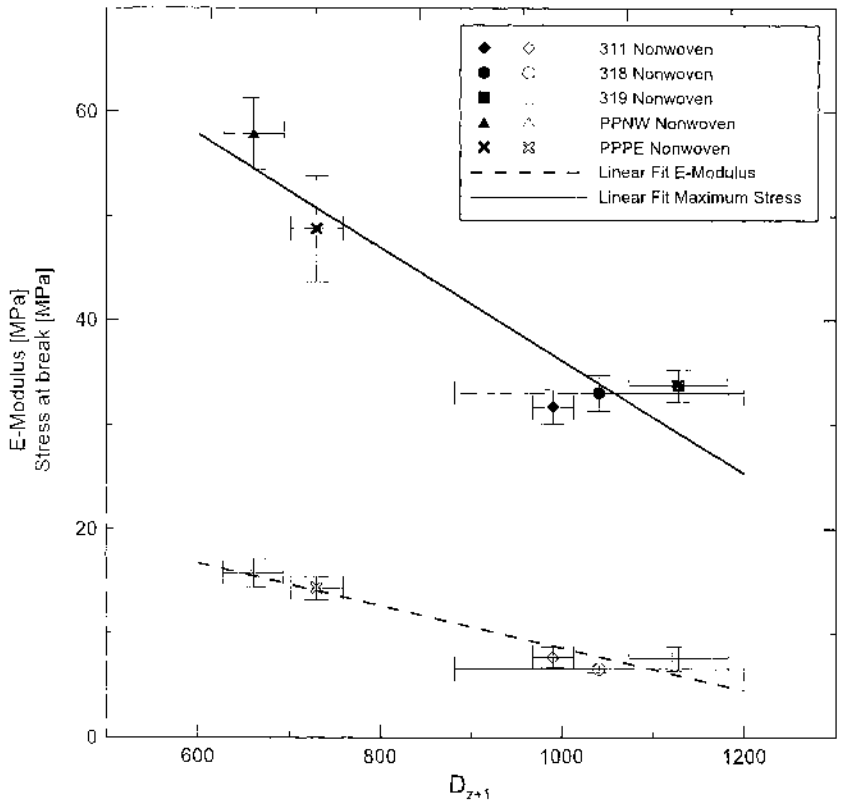

Fig. 14. E-modulus and stress at break as a function of D_{z+1} hole size average.

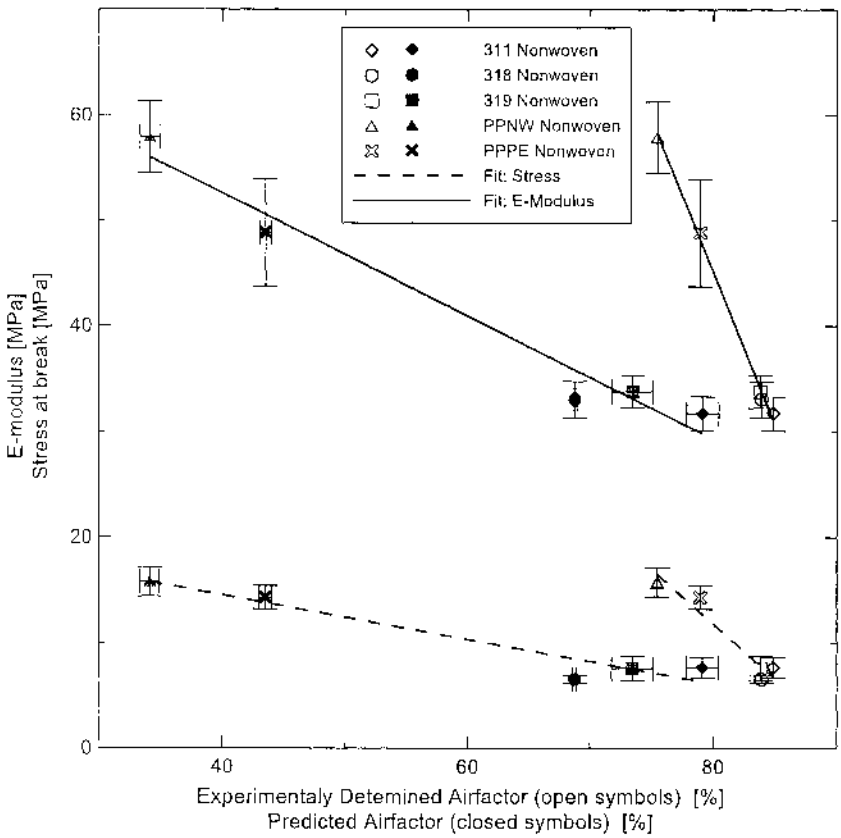

Fig. 15. E-modulus and stress at break as a function of airfactor.

Acknowledgments

The authors wish to acknowledge the Ministry of Education CR for the financial support of grant no. MSM 7088352101.

References

[1] Z.M. Huang, Y.Z. Zhang, M. Kotiki, S. Ramakrishna, Compos. Sei. Technol. 63 (2003) 2223-2253.
[2] M.S. Khil, Di Cha, H.Y. Kim, l.S. Kim, N. Bhattarai, J. Biomed. Mater. 67B (2003) 675-679.
[3] S.H. Kim, Y.S. Nam, T.S. Lee, W.H. Park, Silk, Polym.J. 35 (2003) 185-190.
[4] D. Li, Y. Xia, Adv. Mater. 16 (2004) 1151-1170.
[5] D. Kimmer, P. Slobodian, D. Petras, M. Zatloukal, R. Olejnik, P. Saha, J. Appl. Polym. Sei. Ill (2009) 2711-2714.
[6] T. Uyar, Flemming Besenbacher, Polymer 49 (2008) 5336-5343.
[7] D. Fallahi, M. Rafizadeh, N. Mohammadi, B. Vahidi, Polym. Int. 57 (2008) 1363-1368.
[8] E.P.S. Tan, C.T. Lim, Compos. Sei. Technol. 66 (2006) 1102-1111.
[9] S. Megelski, J.S. Stephens, D.B. Chase, J.F. Rabolt, Macromolecules 35 (2002) 8456.
[10] S. de Vrieze, T. van Camp, A. Nelvig, B. Hagstrom, P. Westbroek, K. de Clerck, J. Mater. Sei. 44 (2009) 1357-1362.
[11] X. Wang, Y. Yan, M.J. Yost, S.A. Fann, S. Dong, X. Li, J. Biomed. Mater. Res. Part A 130-135 (2006).
[12] Lu-Qi Liu, D. Tasis, M. Prato, H.D. Wagner, Adv. Mater. 19 (2007) 1228-1233.
[13] E.P.S. Tan, S.Y. Ng, C.T. Lim, Biomaterials 26 (2005) 1453-1456.
[14] C.L. Casper, J.S. Stehens, N.G. Tassi, D.B. Chase, J.F. Rabolt, Macromolecules 37 (2004) 573-578.
[15] X.F. Wang, X.M. Chen, K.H. Yoon, D.F. Fang, B.S. Hsiao, B. Chu, Environ. Sei. Technol. 39 (2005) 7684-7691.
[16] M.L. Sentmanat, B.N. Wang, G.H. McKinley, J. Rheol. 49 (2005) 585.
[17] M.L. Sentmanat, Rheol. Acta 43 (2004) 657.
[18] M.L. Sentmanat, US Patent No.6, 578, 413, (2003).
[19] M. Ziabari, V. Mottahitalab, A.K. Haghi, Korean J. Chem. Eng. 25 (2008) 923-932.
[20] L. Ghasemi-Mobaralceh, D. Semnani, M. Morshed, J. Appl. Polym. Sei. 106(2007)2536-2542.
[21] D. Semnani, L. Ghasemi-Mobaralceh, M. Morshed, Mohammad- Hossein Nasr-Esfahani, J. Appl. Polym. Sei. Ill (2009) 317—322.